Research Article

Photocatalytic activity of Pr-modified TiO_2 for the degradation of bisphenol A

Denise S. Cordeiro[1] · Fernando L. Cassio[1,2] · Larissa Ciccotti[1] · Thiago L. R. Hewer[1] · Paola Corio[1] · Renato S. Freire[1]

Received: 27 October 2020 / Accepted: 27 January 2021 / Published online: 2 February 2021

Abstract
Praseodymium doped TiO_2 nanoparticles were successfully prepared by the sol–gel method and characterized by X-ray powder diffraction, N_2 adsorption–desorption isotherm, and UV–vis spectroscopy. The effects of the dopant on the crystallite size, specific surface area, average pore diameter, pore volume, and bandgap energy were investigated. The photocatalytic activity of the catalysts was evaluated by bisphenol A degradation and mineralization, which is a representative endocrine disruptor. Furthermore, under visible light irradiation the Pr-modified TiO_2 photocatalysts exhibited higher photocatalytic efficiency than unmodified TiO_2. When praseodymium was loaded (1.0–5.0%) onto the surface of TiO_2, the rates of degradation and mineralization were increased 3–5 times.

Keywords Composite · nanoparticles · Heterogeneous photocatalysis · Praseodymium ion

1 Introduction

Endocrine disrupting chemicals (EDCs) in aquatic systems is a serious environmental problem due to their potential for negative impacts on natural ecosystems and human health. EDCs could cause infertility, feminization, and other adverse effects in the physiological activities of animals derived from unbalance of normal hormonal functions [1, 2]. EDCs include a wide variety of chemicals, such as natural and synthetic hormones, pesticides, personal care products, pharmaceuticals, plasticizers, and several other manufactured products [3, 4]. Among various EDCs, bisphenol A (BPA) is well-known for its interference with the endocrine system. BPA is widely used in the production of multiple items such as epoxy resins, polycarbonate, flame-retardants, and it is also used as a stabilizing agent for many plastics [4–7]. Moreover, BPA is suspected of having carcinogenic effects [8] and it is resistant to biological degradation [9, 10]. Due to its large-scale production and extensive applications, BPA has become an integral part of wastewater streams. Numerous studies have confirmed its presence in rivers, domestic and industrial wastewaters [5, 10]. Thus, it is necessary to improve the treatment systems to prevent its release into the natural waters.

Advanced oxidation processes (AOP) are considered a useful technology for the degradation of persistent environmental pollutants into harmless substances. These processes can completely oxidize organic pollutants to carbon dioxide, water, and inorganic ions [11, 12]. Among a wide range of AOP, heterogeneous photocatalysis has proven to be an effective treatment for water purification. The photocatalytic degradation of organic pollutants has been well described in the literature [11–14]. When a semiconductor is irradiated by light with energy higher than its bandgap, it occurs an electron transition from the valence band to the conduction band. As a result, electron–hole pairs are generated and diffuse out to the surface of the photocatalyst, both of which have high potential enough to produce highly active oxidative species that attack the organic pollutants [13, 14].

✉ Renato S. Freire, rsfreire@iq.usp.br | [1]Instituto de Química, Universidade de São Paulo-USP, São Paulo, SP CEP 05508-000, Brazil. [2]Centro de Ciências Naturais e Humanas, Universidade Federal do ABC, Santo André, SP, Brazil.

TiO_2 is widely used as photocatalyst because it is stable, non-toxic, relatively inexpensive, and presents photoactivity for the degradation of various organic compounds [15, 16]. Although these advantages, there are two main drawbacks to the practical use of TiO_2: the bandgap larger than 3.2 eV, requiring UV light for activation, and the electron–hole recombination rate is too high, resulting in low photo quantum efficiency [13, 16]. Many attempts have been made to enhance the utilization of visible light and to inhibit the recombination electron–hole pairs. The most employed strategies are doping TiO_2-based materials with transition metals and with non-metallic elements [16–18]. Alternatively, the incorporation of lanthanoids ions into TiO_2 could provide better chemical or physical adsorption of organic pollutants due to the ability of lanthanoids ions to form stable complexes with various Lewis bases [19]. Moreover, the TiO_2 modification by lanthanoids ions could also improve the photocatalytic properties due to their effect on the crystal phase, particle size, surface area, and electron–hole pair separation [20–23].

Therefore, the present investigation describes the preparation and characterization of Pr-modified TiO_2 photocatalyst. TiO_2 and Pr-modified TiO_2 were prepared using the sol–gel method. Numerous attempts have been made on the TiO_2 photocatalytic degradation of dyes in water, however much less attention has been paid towards the degradation and mineralization of important contaminants such as BPA. As a part of this investigation, Pr loadings and their effect on bisphenol A degradation and mineralization efficiencies were evaluated.

2 Materials and methods

2.1 Preparation of pure and Pr-modified TiO_2 nanoparticles

Pure TiO_2 and praseodymium-modified TiO_2 were prepared by the sol–gel route [24]. The sol–gel development started from titanium isopropoxide (Acros) and hydrated praseodymium chloride (99.9% Aldrich). All reagents were used without any pre-purification. First, the appropriate amount of $PrCl_3.H_2O$ was dissolved in propanol and mixed with 13 mL titanium isopropoxide. Three different concentrations of praseodymium ions in the titania matrix were evaluated: 1, 3 and 5 wt%. The titanium-praseodymium solution was then added dropwise under vigorous stirring to 200 mL of an aqueous nitric acid solution. Stirring was maintained until a transparent solution was obtained. The transparent sols were dried at 70 °C and calcinated under air at 550 °C for 1 h. Unmodified TiO_2 was synthesized using an identical method without any praseodymium ion addition. All products were kept in desiccators before use.

2.2 Characterization

The chemical, structural, and microstructural features of prepared materials were evaluated using different techniques. Powder X-ray diffraction (XRD) patterns were recorded on a Rigaku X-ray diffractometer equipped whit a Cu tube ($\lambda = 1.5418$ Å). X-ray data were collected at 40 kV, 30 mA, in the range between $5° \le 2\theta \le 90°$ with an angular step size of 0.1° and a count time of 2 s per step. The average crystallite diameters were calculated using Scherrer formula based on the diffraction peak broadening and the full peak width at half the maximum height of the diffraction peak. The mass fractions of anatase, rutile, and brookite phases were calculated from the relationship among the integrated intensities of anatase (101), rutile (110), and brookite, as described by Zhang and Banfield [25]. The cell parameter a was estimated for anatase TiO_2 polymorph using the formula $(1/d = (h^2 + k^2)/a^2/l^2/d^2)$ for tetragonal structure. Scanning electron microscopy (SEM) was carried out with a JEOL SEM-FEG microscopy operated at an accelerating voltage 1.0 kV and a LEI detector. A few droplets of the sample suspended in iso-propylic alcohol were placed on an ITO-glass and drying in vacuum at 70 °C for 12 h. Surface area was determined from nitrogen adsorption–desorption isotherms, using a Quantachrome NOVA 1200e sorptometer. The sorption isotherms were obtained at 77 K, relative pressure from 0.05 to 0.995, and N_2 99.998%. The specific surface areas were determined by the method of Brunauer Emmett Teller (BET). The Barret-Joyner-Halenda (BJH) model was used to determine the pore size distributions. Inductively coupled plasma optical emission spectrometry (ICP-OES) analyses were performed in a Spectro Arcos apparatus. Pr was analyzed at $\lambda = 495.1$ nm. Diffuse reflectance UV–vis spectra were recorded using a Shimadzu UV-2550 spectrometer equipped with an integrating sphere, $BaSO_4$ powder was used as the reflectance standard between 200 and 700 nm.

2.3 Photocatalytic activity

Photocatalysis experiments were carried out in a 500 mL glass cylindrical reactor equipped with a cooling system (25 °C), magnetic stirrer to keep the photocatalyst powder suspended (stirring rate: 500 rpm) and O_2 gas disperser system (200 cm^3 min^{-1}) [26]. The photocatalytic investigation was performed using 225 mg of the photocatalyst dispersed in 300 mL of BPA aqueous solution ([BPA] = 40 mg L^{-1}). The suspension was kept in the dark for 30 min. After the adsorption step in the

dark, the suspension was irradiated using a 125 W high-pressure mercury lamp (Philips), which provided a UV-A light intensity of 2.2 mW cm^{-2}. A UV cut-off Pyrex filter was used as a jacket around the light source to ensure that solution irradiation occurred only form visible light ($\lambda > 400$ nm). At specific intervals, samples where collected, filtered (0.45 µm PTFE membrane filter), and centrifuged at 3500 rpm for 5 min. The supernatant was separated and analyzed. The BPA degradation was evaluated spectrophotometrically ($\lambda = 275$ nm, Shimadzu UV-2550). The BPA mineralization was assessed by total organic carbon (TOC) measurements (Shimadzu 5000A analyzer).

The adsorption behavior of pure TiO_2 and Pr-modified TiO_2 catalysts was investigated using adsorption isotherm tests. Twenty-five milliliters of different BPA solutions, with initial concentrations of 50, 100, 225, 450, and 900 µmol L^{-1}, were placed into 125 mL Erlenmeyer containing 19 mg of the catalysts. All samples were kept 24 h in an orbital table shaker at 180 rpm and 20 °C. The adsorption tests were carried out in dark conditions to avoid any photo effect on BPA degradation. At predetermined times, the catalyst was filtered, and BPA concentrations were measured using a UV–vis spectrometer ($\lambda = 275$ nm, Shimadzu UV-2550). The adsorbed amount of BPA on unmodified TiO_2 or Pr-modified TiO_2 catalysts were calculated based on a mass balance.

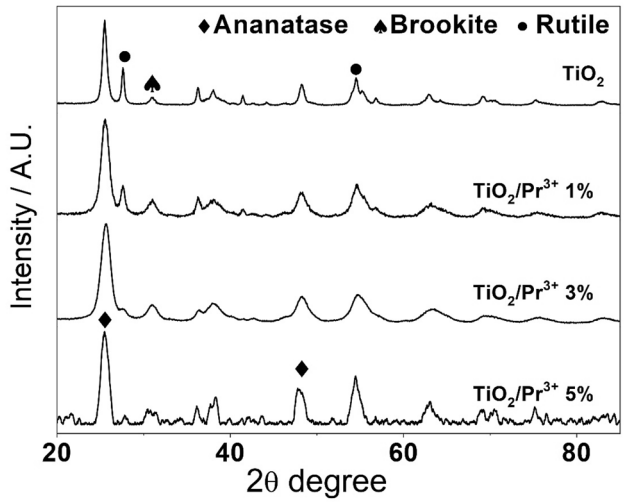

Fig. 1 The XRD patterns of TiO_2 catalyst powders

3 Results and discussion

The X-ray powder diffraction patterns of the raw material and TiO_2 modified with Pr^{3+} ions are shown in Fig. 1. TiO_2 exhibits three crystallographic phases: anatase, rutile and brookite. Anatase phase is a more efficient photocatalyst because of its open structure, compared to rutile phase and the brookite polymorph is generally more reactive than anatase [27]. XRD peaks at $2\theta = 25.5°$ e $2\theta = 48.0°$ were identified as the anatase crystalline form related to planes (101) and (200), respectively. The characteristic diffraction peaks due to rutile crystalline were observed at $2\theta = 27.5°$ (110) and $2\theta = 55.0°$ (211). It was also found a peak at $2\theta = 30.9°$ (121), which is characteristic of the brookite crystalline form [28]. No characteristic diffraction peaks of praseodymium oxides were identified, due to either the crystallites were too small and well distributed around the nanoparticles to be detected or no praseodymium oxides crystalline phases formation occurred. The mass fractions of the TiO_2 phases are shown in Table 1. The preparation method led to the formation of materials composed of a mixture of anatase, rutile, and brookite phases. These allotropes were observed for unmodified and modified TiO_2 samples. The results showed that in the case of the unmodified TiO_2, the anatase phase is the major constituent, followed by rutile and brookite phases. The praseodymium modified TiO_2 catalyst showed the same anatase phase ratio. However, the rutile/brookite ratio was significantly changed. The brookite became the second most abundant phase when praseodymium was present. A slight increase in anatase percentage was observed as a function of Pr^{3+} concentration. Brookite contents were almost independent of Pr concentration. In contrast, the rutile phase ratio decreased with increasing of Pr concentration from 1 to 5%. All TiO_2 phases are reported as photoactive, and the anatase phase is claimed to be the

Table 1 The phase composition and crystallite size of TiO_2 and Pr-modified TiO_2

Sample	Phase composition (%)			Crystallite size (nm)				Constant lattice "a" (Å)	Constant lattice "c" (Å)	Unit Cell volume (Å^3)
	Anatase	Rutile	Brookite	Anatase	Rutile	Brookite	Average			
TiO_2	55 ± 3	28 ± 2	17 ± 2	15.3 ± 0.9	25.8 ± 1.6	14.4 ± 1.3	18.5	3.769	9.251	131.39
TiO_2/Pr^{3+} 1%	50 ± 3	19 ± 2	31 ± 2	8.9 ± 0.8	15.9 ± 1.3	9.2 ± 1.4	11.3	3.769	9.252	131.43
TiO_2/Pr^{3+} 3%	54 ± 3	11 ± 1	35 ± 2	7.3 ± 1.0	18.5 ± 1.5	7.7 ± 1.2	11.2	3.766	9.293	131.78
TiO_2/Pr^{3+} 5%	62 ± 3	7 ± 2	31 ± 2	8.8 ± 1.0	16.7 ± 1.4	5.8 ± 1.3	10.4	3.764	9.282	131.67

most active; indeed, the photocatalytic activity of mixed TiO_2 phases is usually higher than one-phase materials [29, 30]. As well known, rutile is the most stable form, whereas anatase and brookite are metastable, and at high temperatures, these phases are transformed to rutile. Our results suggest that the modifier Pr^{3+} ion stabilized anatase and brookite crystal phase, leading to higher thermal stability [38]. The increased electron density, due to Pr^{3+} presence on the lattice sites, could inhibit the phase transformation in agreement with the literature data [20, 31–33].

Table 1 also gives the average size of the crystalline domains, which were estimated based on the Scherrer equation using anatase (101), rutile (110), and brookite (211) diffraction peaks. The TiO_2 modification seems to lead to a general reduction in the crystallite size for all allotropes. No significant correlation was found between the crystallite size and Pr^{3+} content into modified TiO_2. As observed in other reported literature [32], this reduction could be due to an inhibition of the grain growth by restricting direct contact of the crystallites through the formation of Pr-TiO_2 bonds. It is well known that smaller crystallite sizes provide more stability to the anatase and brookite phases, which is consistent with the phase ratios observed in the Pr-modified TiO_2 [34].

The inhibition of phase transition was ascribed to the stabilization of the anatase phase by the surrounding lanthanide ions through the formation of anatase-O-lanthanide bonds [35]. In the present case, possibly the formation and interaction of Pr–O–Ti takes place and inhibits the phase transition. The possibility of Pr ions placing into the crystalline structure of the TiO_2 by Ti atoms substitution or by its insertion in the interstitial spaces was discarded based in lattice parameters calculations for all catalysts. In Table 1, no significant differences in the lattice parameter were observed in the Pr-modified TiO_2 matrix. The lattice constants a and c were calculated for anatase tetragonal unit cell (which was the crystalline phase more abundant in all materials) and they did not show significant differences for unmodified and modified TiO_2 materials. The same behavior was observed in the unit cell volume values, the volume for unmodified TiO_2 was 131.39 $Å^3$ while for TiO_2/Pr^{3+} 5% was much the same as the unmodified (131.67 $Å^3$). The same effect could be observed in the work conducted by Mazierski et al. [36], in which the authors studied the effect of Er, Yb, Ho, Tb, Gd, Pr doped TiO_2 nanotubes. This could be because the difference in the size of titanium and praseodymium ions which prevents the TiO_2 crystalline structure modification by the lanthanide ion since the radius of Pr^{3+} is much bigger than Ti^{4+} (185 and 88 pm, respectively). In addition, the phase related to Pr could not be observed (Fig. 1), possibly because that Pr could be uniformly dispersed onto TiO_2 nanoparticles, as a small agglomerated of praseodymium oxide. Furthermore, Ti–O–Pr bonds around TiO_2 particles could occur during the process of thermal treatment, inhibiting the formation and growth of crystal nuclei, thereby retarding the phase transition.

SEM was used to further investigate the morphology and the particle size of the samples. As it follows from the SEM images (Fig. 2), the catalyst particles were found to be in amorphous aggregation shape. The Pr^{3+} ion modification does not change neither the agglomeration nor the particle sizes.

Semiconductors with smaller crystallites usually have a more significant number of lattice defects. These defects could enhance the separation and transfer of the photoinduced electron–hole pair [15, 17]. The decrease in crystallite sizes also could increase the total surface area, which provides more active sites for pollutant adsorption and interaction with the photocatalyst surface. Surface area, pore size, and pore size distribution of Pr-modified TiO_2 catalysts were measured by nitrogen adsorption–desorption isotherm using Brunauer–Emmett–Teller (BET) theory.

As shown in Table 2, the Pr-modified TiO_2 catalysts exhibit higher specific surface areas (77–95 $m^2\ g^{-1}$) than unmodified TiO_2 (33 $m^2\ g^{-1}$). The total volume pores were also higher in the Pr-modified materials. The nature and type of the hysteresis loop were categorized based on IUPAC standards [37]. The N_2 adsorption–desorption isotherms presented a hysteresis loop in the region 0.4–0.7 P/P_0, which can be categorized as Type IV isotherm (Fig. 3). The shapes of the hysteresis were of H2 type characterized by mesopores with ink bottle-shaped. The pore size distribution analysis showed dominant mesoporous particles with narrow pore distribution of 1–2 nm. The different surface areas and pore size distributions of Pr-modified and unmodified TiO_2 are expected to cause different results in pollutant adsorption and degradation, as is discussed below.

A set of isothermal adsorption experiments were carried out to evaluate the adsorption of BPA over the catalyst surfaces. The incorporation of the Pr^{3+} ions on the surface of TiO_2 improved the BPA adsorption (Fig. 4). The adsorption capacity of Pr-modified TiO_2 towards BPA was very high, the saturated adsorption amount varied between 70 and 120 mmol g^{-1} for Pr-modified TiO_2 1% and Pr-modified TiO_2 5%, respectively. The BPA adsorption capacity of unmodified TiO_2 was only 20 mmol g^{-1}. Pr^{3+} ions as other lanthanides are known for the ability to form complexes with various Lewis bases, e.g., amines, aldehydes, alcohols, and thiols [38, 39]. These functional groups usually interact with the lanthanides *f* orbitals [40]. The more electrons are available on the analyte (Lewis basicity greater), higher adsorption capacity.

It is well known that the bandgap (Eg) plays a key role in characterizing the photocatalytic properties.

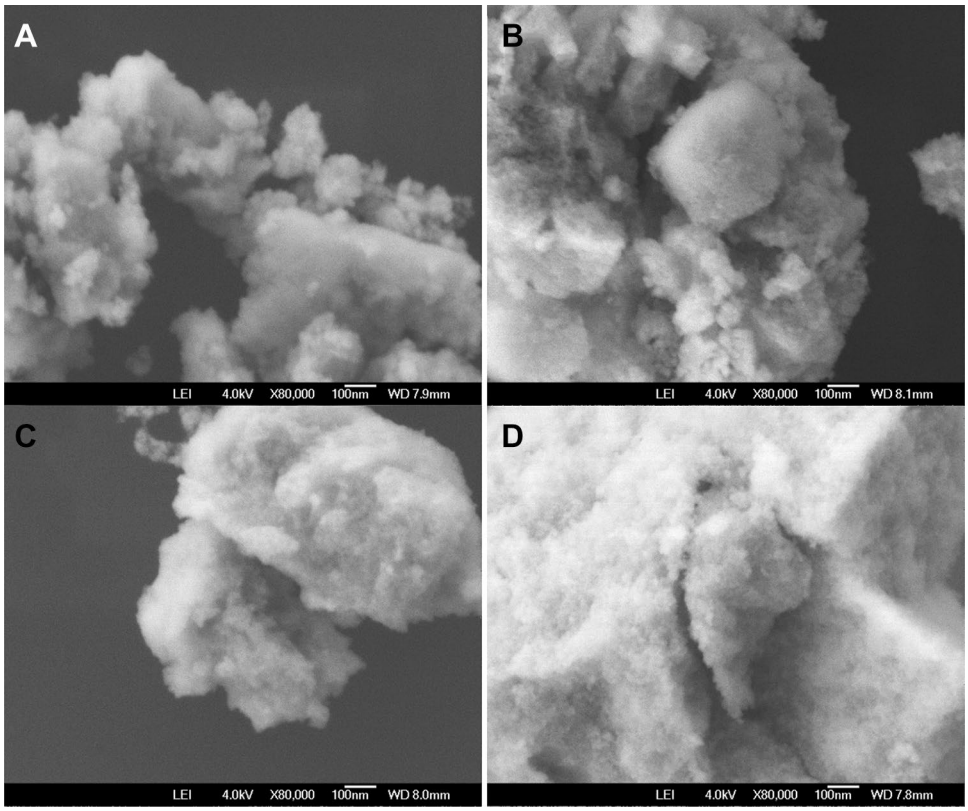

Fig. 2 SEM images of **a** unmodified TiO_2, **b** TiO_2-Pr^{3+} 1%, **c** TiO_2-Pr^{3+} 3% and **d** TiO_2-Pr^{3+} 5%

Table 2 Pore radius, total pore volume, and surface area of Pr-modified and unmodified TiO_2 catalysts

	Pore radius* (nm)	Total pore volume ($cm^3\ g^{-1}$)	Specific surface area*** ($m^2\ g^{-1}$)
TiO_2	1.8	0.05	33
TiO_2/Pr^{3+} 1%	1.7	0.09	78
TiO_2/Pr^{3+} 3%	1.8	0.08	77
TiO_2/Pr^{3+} 5%	1.8	0.13	95

*Obtained from desorption branch

**Obtained by the BJH method

***Calculated by the BET method

The optical absorption of the prepared catalysts was evaluated using UV/Vis diffuse reflectance in the range between 200 and 800 nm (Fig. 5). It is observed that unmodified and Pr-modified TIO_2 samples have substantial absorption at wavelengths below 400 nm, due to transitions of electrons from the valence band to the conduction band of TiO_2. Nevertheless, Pr-modified TIO_2 samples showed four absorption bands between 440 and 590 nm. As reported by Su et al. [20], these peaks can be attributed to the Pr^{3+} 4f transitions $^3H_4 \rightarrow {}^3P_2$, $^3H_4 \rightarrow {}^3P_1$, $^3H_4 \rightarrow {}^3P_0$, $^3H_4 \rightarrow {}^1D_2$ (440, 470, 480 and 590 nm, respectively). Moreover, the absorption intensity was correlated with the Pr^{3+} content.

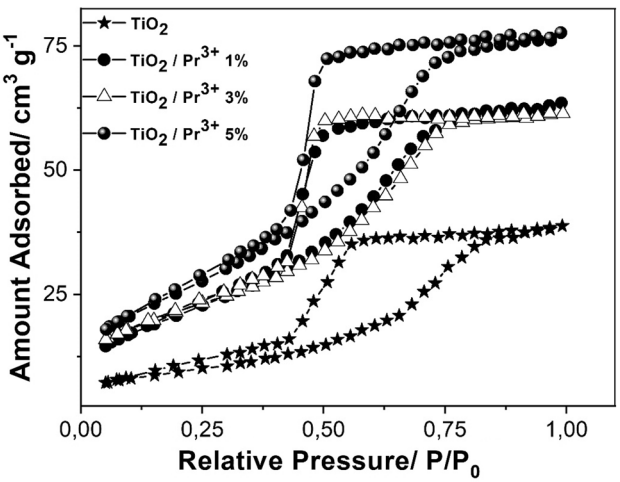

Fig. 3 N_2 sorption isotherms of Pr-modified and unmodified TiO_2 catalysts

The reflectance percentages were transformed using Kubelka–Munk theory, in the form $\left(F\left(R_\infty\right)h\nu\right)^{1/2}$, through the equation $F\left(R_\infty\right) = \frac{1-(\%R)^2}{2(\%R)}$ and subsequent normalization by energy values in eV unit [41]. The estimation of bandgap values (E_g) was made extrapolating the tangent line at the point where the second derivative equals zero (inversion of concavity point) to the x-axis. There was no

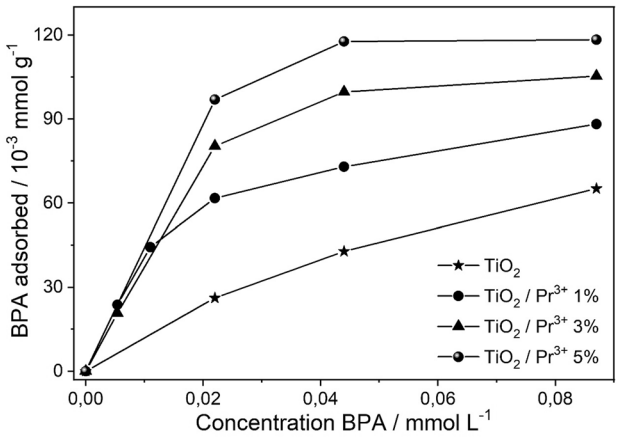

Fig. 4 Adsorption isotherms of BPA on unmodified TiO_2 and Pr-modified TiO_2 catalysts in the dark

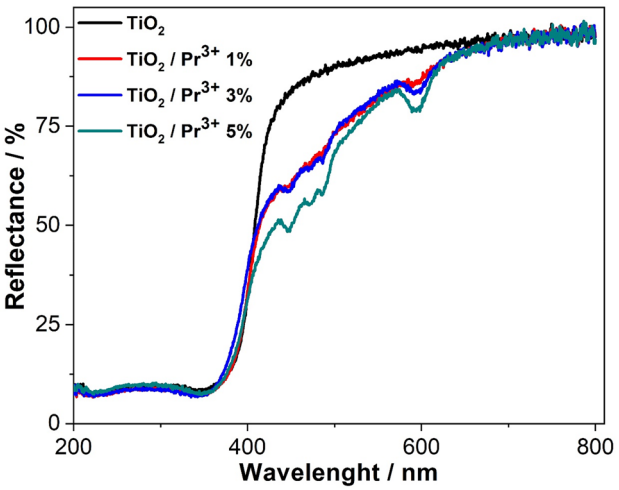

Fig. 5 UV–Vis diffuse reflectance spectra of unmodified TiO_2 and Pr-modified TiO_2

Table 3 The bandgap of unmodified and Pr-modified TiO_2

	E_g (eV)
Unmodified TiO_2	3.02 ± 0.03
TiO_2/Pr^{3+} 1%	2.99 ± 0.03
TiO_2/Pr^{3+} 3%	2.95 ± 0.03
TiO_2/Pr^{3+} 5%	2.92 ± 0.03

statistical difference in the main absorption bandgap energy (Table 3). The slight bandgap shifts as a function of Pr^{3+} content could be attributed to changes in TiO_2 structure and Pr^{3+} light absorption.

Although the Pr^{3+} incorporation into TiO_2 did not change the bandgap energy significantly, trapping migration and separation processes of photogenerated electron–hole pairs could be improved by Pr^{3+} [23, 31–33], which could provide improvement in the photocatalytic activity. Thus, the photocatalytic activity was evaluated by the BPA degradation using visible light irradiation. The photocatalytic ability of Pr-modified and unmodified TiO_2 under the same experimental conditions is shown in Fig. 6. Pr-modified TiO_2 catalysts exhibited significantly enhanced photoactivity for BPA degradation compared with unmodified TiO_2. The photocatalytic efficiency of Pr-modified TiO_2 was improved by 2.5 folds as compared to unmodified TiO_2 after 180 min of treatment. Notably, the modified catalyst demonstrated excellent ability to mineralize BPA, in which the TOC reduction was 3 times greater than unmodified TiO_2 after 90 min of treatment.

After each photocatalytic activity evaluation, the amount of praseodymium ions in the supernatant was analyzed by ICP. The concentration of leached Pr ions was negligible during the photocatalytic process. TiO_2 modified with Pr^{3+} 1% showed the highest photocatalytic efficiency for BPA degradation and mineralization. No significant differences in the BPA degradation were observed with different dosages of the lanthanide ion. On the other hand, the photocatalytic mineralization efficiency showed a slight decrease with the increase of Pr concentration. Since Pr^{3+} also can play a role as trapping sites for both holes and electrons, the ability of charge carriers trapping increases at higher modifier concentration [40, 42, 43]. The dispersion of praseodymium oxides onto the surface of TiO_2 also led to an increase in the surface area. Moreover, the modifier Pr^{3+} ion stabilized anatase and brookite crystal phase, leading to higher thermal stability, as well known anatase and brookite phases are more photocatalytic active than rutile. At the same time, smaller particles favor a faster movement of photoexcited carriers to the surface of TiO_2 during the catalytic process, which also can contribute to less photogenerated carrier recombination.

4 Conclusion

In this research, a simple one-step method to produce Pr-modified TiO_2 with photocatalytic activity was described. The addition of praseodymium ions on the TiO_2 structure, significantly influences the crystallization phases, stabilized anatase and brookite crystal phase, leading to higher thermal stability. The XDR results showed that the crystal size significantly decreased due to lanthanide ion presence, but an increase in specific surface area was observed. Praseodymium ions play an essential role in improving the surface textural properties and further increases the BPA adsorption capacity. The modified TiO_2 adsorption capacity was proportional to the praseodymium loading. On the other hand, no significant shifting in the absorption edge to the visible region and reduction of the bandgap was

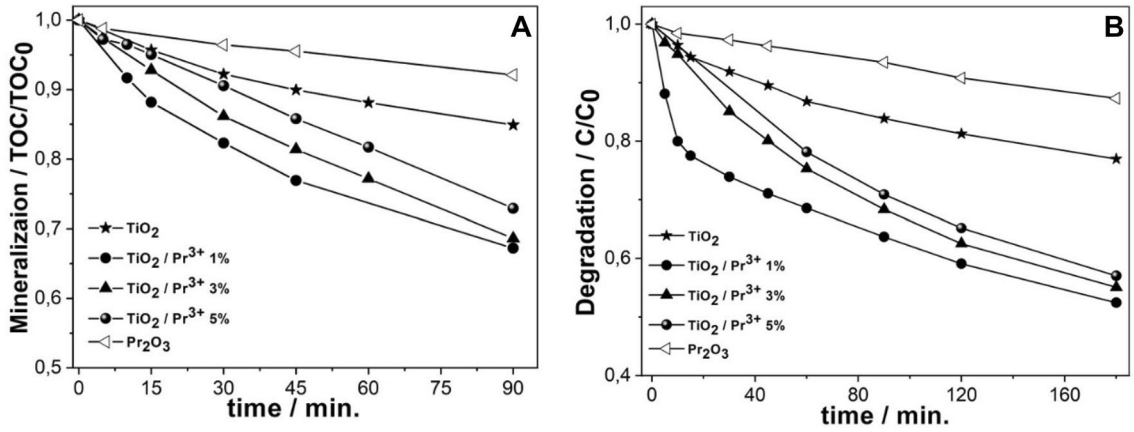

Fig. 6 Mineralization (**a**) and degradation (**b**) of BPA as a function of photocatalytic treatment using Pr_2O_3; unmodified TiO_2 and Pr-modified TiO_2 with different loading amounts of Pr deposited. Catalysts mass = 0.75 g L^{-1}; $[BPA]_0$ = 40 mg L^{-1}

observed due to the presence of Pr. The Pr-modified TiO_2 catalyst exhibited excellent photocatalytic activity, under visible light irradiation, for both BPA degradation and mineralization, presenting higher activity than unmodified TiO_2. The optimum Pr^{3+} loading found in this study was between 1.0 wt%. Under these conditions, the efficiency of BPA degradation was 2.5 times higher than the unmodified TiO_2 photocatalysts. The activity could be due to both the increase of adsorption ability and the enhancement of electron–hole pairs separation, which was attributed to the presence of a suitable amount of Pr^3. The experiments described here demonstrate the feasibility of a simple preparation of Pr-modified TiO_2 with high photoactivity for BPA degradation and mineralization using visible light irradiation.

Acknowledgements The authors would like to thank CNPq, Capes and FAPESP for financial supports to this work.

Compliance with ethical standards

Conflict of interest The authors have declared no conflict of interest.

References

1. Sharma A, Mollier J, Brocklesby RWK, Caves J, Jayasena CN, Minhas S (2020) Endocrine-disrupting chemicals and male reproductive health. Reprod Med Biol 19:243
2. Selvaraju V, Baskaran S, Agarwal A, Henkel R (2020) Environmental contaminants and male infertility: Effects and mechanisms. Andrologia 5:e13646
3. Kim JJ, Kumar S, Kumar V, Lee YM, Kim YS, Kumar V (2020) Bisphenols as a Legacy Pollutant, and their effects on organ vulnerability. Int J Environ Res Public Health 17:112
4. Su C, Cui Y, Liu D, Zhang H, Baninla Y (2020) Endocrine disrupting compounds, pharmaceuticals and personal care products in the aquatic environment of China: which chemicals are the prioritized ones? Sci Total Environ 720:137652
5. Abraham A, Chakraborty P (2020) A review on sources and health impacts of bisphenol A. Rev Environ Health 35:201
6. Akash MSH, Sabir S, Rehman K (2020) Bisphenol A-induced metabolic disorders: from exposure to mechanism of action. Environ Toxicol Phar 77:103373
7. Gonsioroski A, Mourikes VE, Flaws JA (2020) Endocrine disruptors in water and their effects on the reproductive system. Int J Mol Sci 21:1929
8. Nomiri S, Hoshyar R, Ambrosino C, Tyler CR, Mansouri B (2019) A mini review of bisphenol A (BPA) effects on cancer-related cellular signaling pathways. Environ Sci Pollut Res 26:8459
9. Ahmed MB, Zhou JL, Ngo HH, Guo W, Thomaidis NS, Xu J (2017) Progress in the biological and chemical treatment technologies for emerging contaminant removal from wastewater: a critical review. J Hazard Mater 323:274
10. Wang H, Liu ZH, Zhang J, Huang RP, Yin H, Dang Z, Wu PX, Liu Y (2019) Insights into removal mechanisms of bisphenol A and its analogues in municipal wastewater treatment plants. Sci Total Environ 692:107
11. Ghatak HR (2014) Advanced oxidation processes for the treatment of biorecalcitrant organics in wastewater. Crit Rev Environ Sci Tech 44:1167
12. Oturan MA, Aaron JJ (2014) Advanced oxidation processes in water/wastewater treatment: principles and applications. a review. Crit Rev Environ Sci Tech 44:2577
13. Konstantinou IK, Albanis TA (2004) TiO2-assisted photocatalytic degradation of azo dyes in aqueous solution: kinetic and mechanistic investigations. Appl Catal B Environ 49:1

14. Khki MRD, Shafeeyan MS, Raman AAA, Daud WMAW (2017) Application of doped photocatalysts for organic pollutant degradation—a review. J Environ Manage 198:78
15. X. Chen, X S.S Mao, Chem. Rev. **2007**, 107, 2891.
16. Chen DJ, Cheng YL, Zhou N, Chen P, Wang YP, Li K, Huo SH, Cheng PF, Peng P, Zhang RC, Wang L, Liu H, Liu Y, Ruan R (2020) Photocatalytic degradation of organic pollutants using TiO2-based photocatalysts: a review. J Clean Prod 268:121725
17. Karthikeyan C, Arunachalam P, Ramachandran K, Al-Mayouf AM, Karuppuchamy S (2020) Recent advances in semiconductor metal oxides with enhanced methods for solar photocatalytic applications. J Alloys Compd 828:154281
18. Li RX, Li T, Zhou QX (2020) Impact of titanium dioxide (TiO2) modification on its application to pollution treatment—a review. Catalysts 10:804
19. Saif M, Abdel-Mottaleb MSA (2007) Titanium dioxide nanomaterial doped with trivalent lanthanide ions of Tb, Eu and Sm: Preparation, characterization and potential applications. Inorganica Chim Acta 360:2863
20. Su W, Chen J, Wu L, Wang X, Wang X, Fu X (2008) Visible light photocatalysis on praseodymium(III)-nitrate-modified TiO2 prepared by an ultrasound method. Appl Catal B Environ 77:264
21. Xu A-W, Gao Y, Liu H-Q (2002) The preparation, characterization, and their photocatalytic activities of rare-earth-doped TiO2 nanoparticles. J Catal 207:151
22. Mazierski P, Mikolajczyk A, Bajorowicz B, Malankowska A, Zaleska-Medynska A, Nadolna J (2018) The role of lanthanides in TiO2-based photocatalysis: a review. Appl Catal B Environ 233:301
23. Li FB, Li XZ, Ao CH, Lee SC, Hou MF (2005) Enhanced photocatalytic degradation of VOCs using Ln3+–TiO2 catalysts for indoor air purification. Chemosphere 59:787
24. Hewer TLR, Souza ECC, Martins TS, Muccillo ENS, Freire RS (2011) Influence of neodymium ions on photocatalytic activity of TiO2 synthesized by sol–gel and precipitation methods. J Mol Catal A Chem 336:58
25. Zhang H, Banfield JF (2000) Understanding polymorphic phase transformation behavior during growth of nanocrystalline aggregates: insights from TiO_2. J Phys Chem B 104:3481
26. Hewer TLR, Machado BC, Freire RS, Guardani R (2014) Ag_3PO_4 sunlight-induced photocatalyst for degradation of phenol. RSC Adv 65:34674
27. Velardi L, Scrimieri L, Serra A, Manno D, Calcagnile L (2020) Effect of temperature on the physical, optical and photocatalytic properties of TiO_2 nanoparticles. SN Appl Sci 2:707
28. Bergamonti L, Alfieri I, Lorenzi A, Montenero A, Predieri G, Di Maggio R, Girardi F, Lazzarini L, Lottici PP (2015) Characterization and photocatalytic activity of TiO2 by sol–gel in acid and basic environments. J Sol-Gel Sci Technol 73:91
29. Bakardjieva S, Stengl V, Szatmary L, Subrt J, Lukac J, Murafa N, Niznansky D, Cizek K, Jirkovsky J, Petrova N (2006) Transformation of brookite-type TiO2 nanocrystals to rutile: correlation between microstructure and photoactivity. J Mater Chem 16:1709
30. Katal R, Masudy-Panah S, Tanhaei M, Farahani MHDA, Hu JY (2020) A review on the synthesis of the various types of anatase TiO2 facets and their applications for photocatalysis. Chem Eng J 384:123384
31. Romero DD, Torres G, Arevalo JC, Gomez R, Aguilar-Elguezabal A (2010) Synthesis and characterization of TiO2 doping with rare earths by sol–gel method: photocatalytic activity for phenol degradation. J Sol-Gel Sci Technol 56:219
32. Yang J, Dai J, Li J (2011) Synthesis, characterization and degradation of Bisphenol A using Pr, N co-doped TiO2 with highly visible light activity. Appl Surf Sci 257:8965
33. Luo W, Hou JL, Zou DH, Cui LN, Zhu QY, Dai J (2018) Lanthanide–titanium-oxalate clusters and their degradation products, photocurrent response and photocatalytic behaviours. New J Chem 42:11629
34. Li W-K, Hu P, Lu G, Gong X-Q (2014) Density functional theory study of mixed-phase TiO2: heterostructures and electronic properties. J Mol Model 20:2215
35. Arbiol J, Cerda J, Dezanneau G, Cirera A, Peiro F, Cornet A, Morante JR (2002) Effects of Nb doping on the TiO_2 anatase-to-rutile phase transition. J Appl Phys 92:853
36. Mazierski P, Lisowski W, Grzyb T, Winiarski MJ, Klimczuk T, Mikołajczyk A, Flisikowski J, Hirsch A, Kołakowska A, Puzyn T, Zaleska-Medynska A, Nadolna J (2017) Enhanced photocatalytic properties of lanthanide-TiO_2 nanotubes: an experimental and theoretical study. Appl Catal B Environ 205:376
37. Sotomayor FJ, Cychosz KA, Thommes M (2018) Characterization of micro/mesoporous materials by physisorption: concepts and case studies. Acc Mater Surf Res 3:34
38. Plecnik CE, Liu SM, Shore SG (2003) Lanthanide–transition-metal complexes: from ion pairs to extended arrays. Acc Chem Res 36:499
39. Bunzli JCG (2015) On the design of highly luminescent lanthanide complexes. Coord Chem Rev 293:19
40. Ranjit KT, Willner I, Bossmann SH, Braun AM (2001) Lanthanide oxide doped titanium dioxide photocatalysts: effective photocatalysts for the enhanced degradation of salicylic acid and t-Cinnamic acid. J Catal 204:305
41. Christy AA, Kvalheim OM, Velapoldi RA (1995) Quantitative analysis in diffuse reflectance spectrometry: a modified Kubelka-Munk equation. Vib Spectrosc 9:19
42. Choi W, Termin A, Hoffmann MR (1994) The role of metal ion dopants in quantum-sized TiO2: correlation between photoreactivity and charge carrier recombination dynamics. J Phys Chem 98:13669
43. Liang C-H, Li F-B, Liu C-S, Lü J-L, Wang X-G (2008) The enhancement of adsorption and photocatalytic activity of rare earth ions doped TiO2 for the degradation of Orange I. Dyes Pigm 76:477